Fractality-induced topological phase squeezing and devil's staircase

Junkai Li,[1,*] Yeyang Sun,[1,*] Qingyang Mo,[1] Zhichao Ruan,[1,2,†] and Zhaoju Yang[1,†]

[1]*Department of Physics, Interdisciplinary Center for Quantum Information, Zhejiang Province Key Laboratory of Quantum Technology and Device, Zhejiang University, Hangzhou 310027, Zhejiang Province, China*

[2]*State Key Laboratory of Modern Optical Instrumentation, Zhejiang University, Hangzhou 310027, Zhejiang Province, China*

(Received 7 October 2022; accepted 9 May 2023; published 26 June 2023)

We propose and experimentally demonstrate the first example of Chern fractal insulators in an acoustic Sierpinski lattice. Through introducing fractality into the well-known Haldane model, we find that the topological phase diagram is significantly squeezed by about 0.5 times, compared with that of the original Haldane model. The energy spectra for different generations of a fractal lattice exhibits a hierarchy of self-similar energy bands in the form of a devil's staircase. With local acoustic measurements, we fabricate the sonic sample based on the theoretical model and experimentally confirm the fractality-induced squeezing and observe the one-way edge states that are protected by a robust mobility gap. Our work demonstrates the fundamental interplay between the fractality and topological Haldane insulator, and may provide new directions for the advanced control of sound waves.

DOI: 10.1103/PhysRevResearch.5.023189

I. INTRODUCTION

Topological insulators [1,2] with the distinctive characteristics of an insulating bulk and conducting edge states reveal a topologically distinct phase of matter that cannot be described by Landau's theory of phase transitions. One important class of topological systems is the Chern insulator or quantum anomalous Hall effect, which has integer Hall conductivity and no Landau levels. In 1988, Haldane [3] presented a paradigmatic example of a Chern insulator on a honeycomb lattice with staggered magnetic flux but a net magnetic field of zero. This topological Haldane model utilizes both time-reversal and inversion symmetry breaking to open a bandgap at Dirac points. The competition between the two broken symmetries results in topologically nontrivial and trivial phases, which can be characterized by Chern numbers [4]. While the experimental realizations of the electronic Chern insulators were challenging [5,6], a photonic version of the Chern insulator was proposed by Haldane and Raghu [7] in 2008 and experimentally observed with microwaves in a gyromagnetic photonic crystal [8,9] shortly thereafter, which opened the door to exploring topological physics in the classical wave systems [10–14], including acoustics [15–25]. The acoustic waves cannot respond to the external magnetic field and have no spin. Therefore, the realization of acoustic Chern insulators was not that straightforward dating back to 10 years ago. With the help of breaking of the time-reversal symmetry [19], acoustic topological insulators were proposed based on the artificial gauge fields induced by circulating airflows [15,16,20]. However, the complex engineering of the circulating flow is challenging for experiments. In parallel, another proposal showed that the staggered magnetic flux in the two dimensions can be constructed by introducing the chiral couplings in an additional third dimension [17]. With this method, the acoustic analogue of the topological Haldane model was directly mapped and experimentally realized [21,22] later on. Since then, many ideas have been proposed along these veins based on artificial gauge fields and lattice symmetries. Nowadays, the acoustic system has become a feasible platform for exploring various topological states [23,24,26] in integer dimensions ranging from the quantum Hall effect [15,16] to the quantum spin Hall effect [27,28], valley Hall effect [29], Weyl and Dirac semimetals [21,22,30], high-order topological insulators [31–37], non-Abelian topological insulators [38–40], and to aperiodic topological quasicrystals [41].

On the other hand, recent theoretical proposals show that the topological states can even go beyond the integer dimensions and exist in the fractal lattices [42–47]. Fractals appearing the same at different scales are characterized by fractal dimensions, self-similarity, and scale invariance [48,49]. They do not have a well-defined bulk like the integer-dimensional crystals, and yet they are able to support topological edge states. Despite the increasing interest in topological fractal insulators, their experimental realization is not straightforward and an early attempt [50] revealed that the fractality would turn off the topological properties. Until recently, it has been reported that the Floquet topological states were realized in a Sierpinski photonic fractal lattice consisting of helical waveguides [46,51]. These advances, both in condensed matter and photonics, have changed the current understanding of bulk-edge correspondence: the topo-

*These authors contributed equally to this work.
†zhichao@zju.edu.cn, zhaojuyang@zju.edu.cn

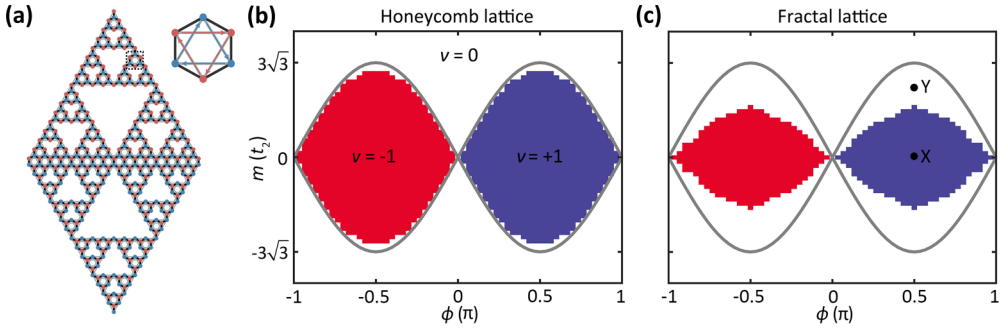

FIG. 1. Topological phase diagram of the honeycomb and fractal lattices. (a) A schematic of the fractal Haldane model that is composed of two Sierpinski gaskets. Red and blue dots indicate A and B sublattices with the same number of sites. The NN and NNN couplings are represented by black and gray lines. The NNN hopping along the red or blue arrows can accumulate a phase of ϕ. The inset is an enlarged view of a hexagonal cell. (b) Topological phase diagram of the rhombic honeycomb lattice. In the original Haldane model, topological phase transitions obey $|m| = |3\sqrt{3}t_2 \sin\phi|$, which is marked by gray lines. The Bott indexes of 0, $+1$, and -1 are represented by white, blue, and red, respectively. (c) The phase diagram of the fractal lattice is significantly squeezed by about 0.5 times along the vertical axis m. The coupling parameters for theoretical calculations are $t_1 = 1, t_2 = 0.2$.

logical properties do not necessarily rely on the internal bulk. However, thus far, little topological fractal physics has been demonstrated, and the interplay between the topological phase diagram and fractality still remains poorly understood.

Here we present and demonstrate the squeezed Chern insulator in an acoustic fractal system. We begin with a fractal lattice consisting of two Sierpinski gaskets with the same number of A- and B-sites. By calculating the phase diagram based on the real-space Bott index [52,53], we find that the topological phase diagram is squeezed by about 0.5 times, compared with that of the original Haldane model. The energy spectra for different generations of topological fractal lattices exhibit a hierarchy of self-similar energy bands in the form of a devil's staircase [54]. Importantly, we show that contrary to conventional topological insulators, there exists a robust mobility gap in our fractal model protecting the topological edge states instead of the direct bandgaps. In experiments, we observe the squeezing effect on the phase diagram and investigate the dynamics of the topological edge states. We show that sound waves can propagate along the outer and inner edges without penetrating into the interior of the lattice and backscattering in the presence of corners and defects. Counterintuitively, we find the topological protection can be preserved along the solely single-atom path around the defect.

II. NUMERICAL CALCULATION

Our starting point is a fractal Haldane model [Fig. 1(a)] consisting of two Sierpinski gaskets with a fractal dimension [48] of $d_f = \frac{\ln(3)}{\ln(2)} \approx 1.585$, which is calculated from the box-counting method. More detail can be found in Supplementary Material Sec. 1 [55]. The Hamiltonian of the system can be written as

$$H = \sum_{\langle ij \rangle} t_1 c_i^\dagger c_j + \sum_{\langle\langle ij \rangle\rangle} t_2 e^{i\phi_{ij}} c_i^\dagger c_j + m\left(\sum_{i\in A} c_i^\dagger c_i - \sum_{i\in B} c_i^\dagger c_i\right), \tag{1}$$

where $c_i^\dagger$ ($c_{i,j}$) is the creation (annihilation) operator, t_1 and t_2 are nearest-neighbor (NN) and next-nearest-neighbor (NNN) coupling strength, ϕ_{ij} is the phase accumulation when hopping from site j to NNN site i, and m denotes the onsite energy difference between sites A and B. The time-reversal and inversion symmetry can be broken by changing ϕ and m, respectively. In the original Haldane model, the competition between the two broken symmetries can give rise to the topological phase transition [marked by the gray lines in Fig. 1(b) and 1(c)]. Intuitively, one may wonder whether there is a topological phase transition in our fractal system and where the phase transition is.

To verify that the topological phase transition indeed exists in our fractal model, we need to characterize the system by the topological invariant. Unfortunately, there is no well-defined topological index in the fractal dimensions due to the fragmented space and the lack of translation symmetry. Therefore, we have to project the fractal lattice onto a two-dimensional space and resort to an alternative invariant—the Bott index [52,53]. The results of the Bott index (see details in Supplemental Material Sec. 5 [55]) as a function of ϕ and m are shown in Fig. 1(b) and 1(c). For a direct comparison, we obtain the Bott index diagram for both the honeycomb [Fig. 1(b)] and our fractal lattice [Fig. 1(c)]. The well-known topological transition governed by $|m| = |3\sqrt{3}t_2 \sin\phi|$ in the Haldane model is marked by gray lines, as shown in both panels. These lines connect two regimes with a different Chern number ν changing from 0 to $+1$ or to -1. For the honeycomb lattice [Fig. 1(b)], the phase diagram calculated from the Bott index is consistent with that calculated from the Chern number. The Bott indexes of 0, $+1$, and -1 are represented by white, blue, and red, respectively. The transition between the Bott indexes of ± 1 and 0 overlaps with the theoretical prediction (gray lines). For the fractal lattice, the phase diagram [Fig. 1(c)] is significantly squeezed by about 0.5 times along the vertical axis m, which is due to the reduction in the number of lattice sites that require less intense inversion symmetry breaking to balance the time-reversal symmetry breaking. The phase diagrams of the different fractal generations are shown in Supplemental Material Sec. 6, Fig. S6 [55] to examine the validity of the diagram squeezing. These transitions are consistent with that calculated from the real-space Chern numbers

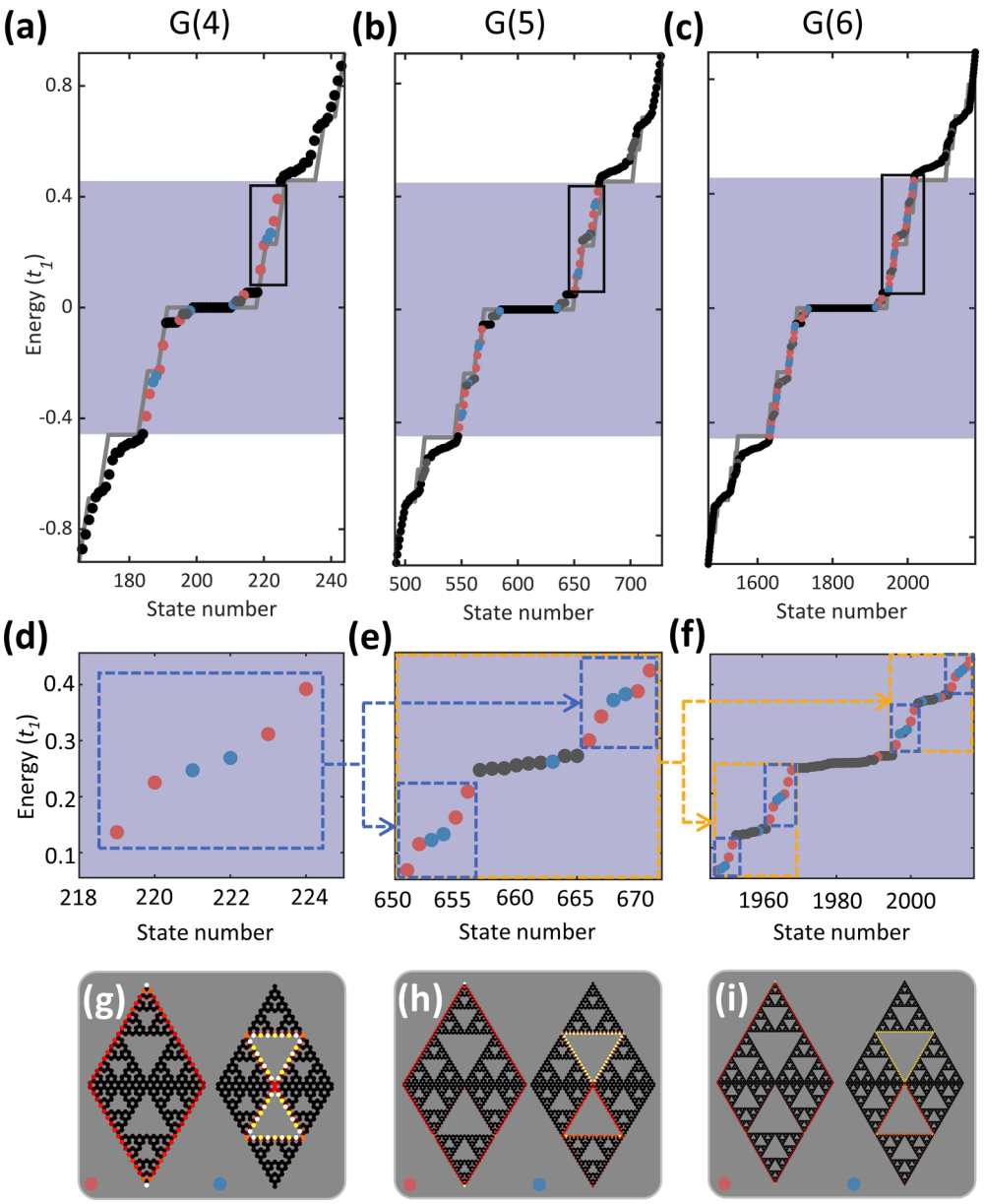

FIG. 2. Devil's staircase and edge states in the fractal lattices. (a)–(c) Energy spectra for the topological fractal lattices of G(4) to G(6). Red and blue dots indicate the external and dominant internal edge states. Gray dots correspond to a hierarchy of internal edge states localized at the perimeters of various voids. The blue shaded region indicates the topological bandwidth, where the topological transmission can be supported. The edge states in the black boxes in (a)–(c) iterate over the devil's staircase, shown as gray curves. (d)–(f) The enlarged views of the black boxes shown in (a)–(c). The blue and yellow dashed boxes in (d)–(f) double themselves at the next iterative generation of the fractal lattice. (g)–(i) The field patterns of the edge states localized at the external and dominant internal edges (Supplemental Material Videos S1 and S2). The external (internal) edge states have the state number of 224, 666, 2011 (222, 654, 1950).

(see Supplemental Material Sec. 7 [55]). Note that despite the existence of topological phase transitions, the maximum size of the topological bandgap for the fractal model is about 65% of that in the honeycomb lattice (Supplemental Material, Sec 8 [55] for details), which indicates the relatively weaker strength of topological protection (Supplemental Material Sec. 10 [55]). In Supplemental Material Sec. 11 [55], we further unravel that the phase transition in our model is fundamentally distinct from the honeycomb lattice with randomly missed sites.

Having found there exists a topological phase transition in the fractal model and the phase diagram is squeezed significantly, we calculate the eigenvalues and eigenstates at point X (nontrivial) for fractal lattices with $\phi = \frac{\pi}{2}$, $m = 0$. Point X is labeled in Fig. 1(c). The energy spectra for generations of G(4) to G(6) are shown in Figs. 2(a)–2(c). In the energy spectra, the red and blue dots indicate the external and dominant internal edge states, as shown in Figs. 2(g)–2(i). The gray dots correspond to a hierarchy of internal edge states and hybrid states localized at the perimeters of various voids

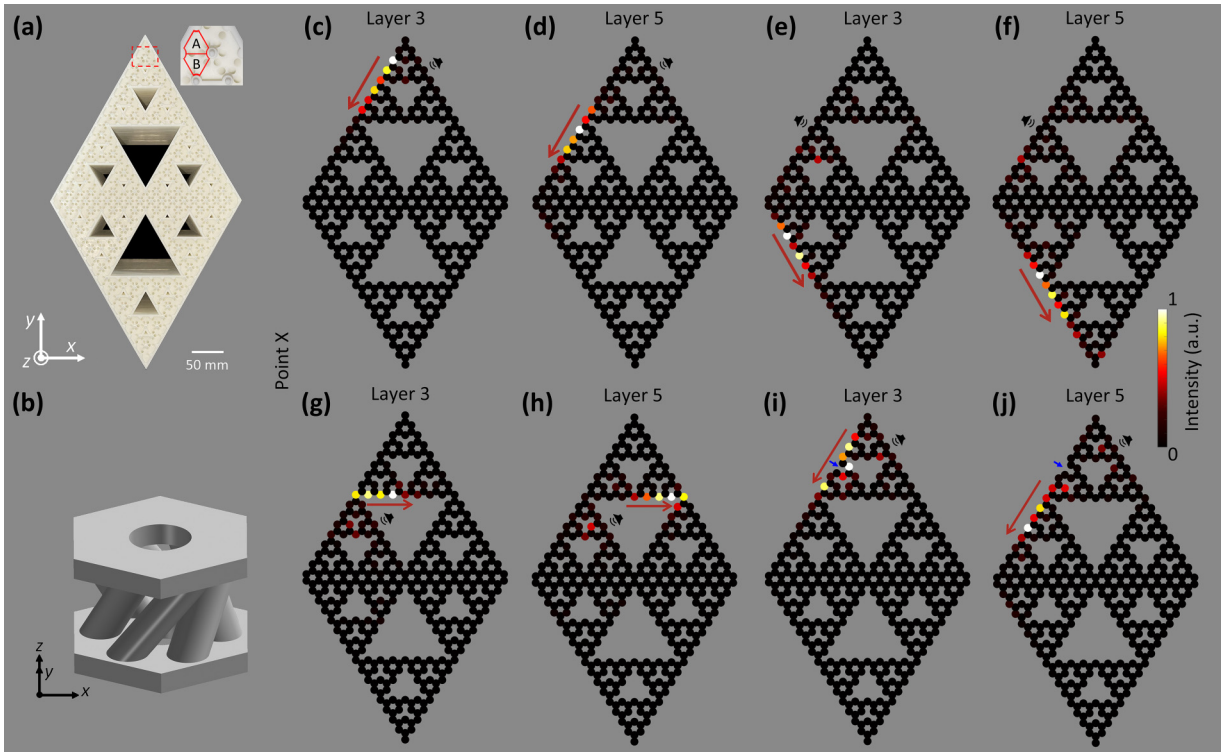

FIG. 3. Observation of the fractal topological edge states. (a) Photo of the acoustic sample. The inset shows an enlarged view of A and B meta-atoms. (b) Structure of the acoustic hexagonal cell, which is periodic along the z-axis and can be mapped onto the hexagonal cell in Fig. 1(a). The complex NNN hopping is introduced by adding chiral tubes. An effective staggered magnetic flux can be included at a fixed momentum k_z [$\phi = k_z d_z \in (0, \pi)$]. (c) and (d) Sound intensity distribution of the external topological edge states after three- and five-layer propagation. (e) and (f) Moving the sound source leftward makes the acoustic wave propagate through the obtuse corner and farther down along the edge. (g) and (h) Intensity distribution of the internal topological edge states after three- and five-layer propagation. (i) and (j) Intensity distribution of the edge states after three- and five-layer propagation in the presence of a defect, indicated by blue arrows. Note that the topological systems in this figure correspond to point X in Fig. 1(c). The red arrows point out the direction of the sound propagation.

(see Supplemental Material Sec. 3 [55] for more details) that arise from the iterative generation of the fractal geometry. The appearance of the internal edge states, in turn, makes the fractal topological insulator consist entirely of "edges" and no "bulk" [46,51]. Moreover, these abundant internal boundary states can make their dimensionality consistent with the lattice dimension [56]. In this work, these internal edge states allow the energy spectrum to form a devil's staircase. The iterative generations of the fractal lattices can give rise to more and more topological edge states (blue, red, and dark-gray dots) that fill up the energy intervals and generate new staircases. For example, in the G(5) lattice, the yellow dashed box [Fig. 2(e)] encompasses energies from 0.08 to 0.42. It includes one longer staircase inherited from the G(4) lattice [Fig. 2(d)], with an energy close to 0.28, as well as two new staircases generated during the iteration, with energies close to 0.12 and 0.38, respectively. The nearly flat, long staircase connecting different dashed boxes includes a lot of internal edge states localized at the perimeters of various interior voids. The dashed boxes in Figs. 2(d)–2(f) with the same color share the similar spectrum distribution of topological edge states. Importantly, we can see that the spectra exhibiting a hierarchy of self-similar staircases can be fitted into a form of a devil's staircase [48,54] [see gray lines in Figs. 2(a)–2(c) and Supplemental Material Sec. 12 [55] for details], which is continuous everywhere and has a zero derivative everywhere, but its value is still monotonically increasing.

III. EXPERIMENTAL OBSERVATION

As we know, the topological edge states only reside in the bandgap in conventional topological insulators. However, the topological propagation in our fractal model can even survive in the presence of the trivial states with the energy close to zero (see Supplemental Material Videos S3 to S5 [55]). The reason is, because of the lack of the well-defined bulk, there is negligible coupling between the edge states and the states localized at the perimeters of the interior voids. Therefore, there exists a robust mobility gap ranging from -0.46 to 0.46 [blue shaded region in Figs. 2(a)–2(c)] corresponding to a Bott index of $+1$ that protects the topological edge states instead of the direct bandgaps, which makes our fractal model fundamentally distinct from the conventional topological band insulator. Note that in Supplemental Material Video S6 [55], we also show the topological transport survives as long as the perimeter of the edge encloses an area that is larger than G(2). Due to the finite-size effect, the edge enclosing a smaller area cannot support one-way transport.

To demonstrate experimentally the topological edge states in the fractal system, we design and fabricate a synthetic

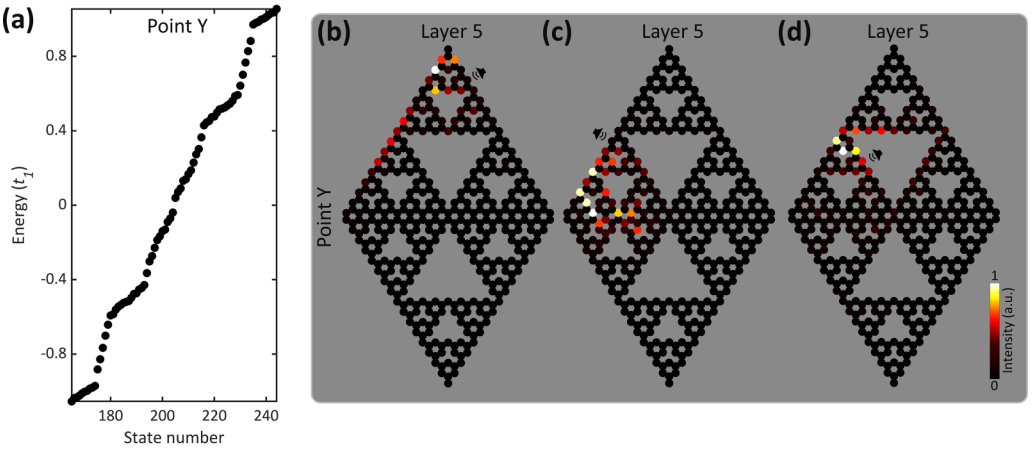

FIG. 4. The trapped sound in the trivial phase. (a) The energy spectrum for the trivial states, which correspond to point Y as labeled in Fig. 1(c). (b) and (c) Sound intensity distribution of the acoustic wave after five-layer propagation. It can be seen that the sound waves are clearly trapped. (d) Intensity distribution of the acoustic wave after five-layer propagation. We can see that the acoustic waves cannot propagate along the edges and bypass the corners, compared with that in Fig. 3(h). The schematic speakers indicate the positions of the source array that emits acoustic waves with a frequency of 10 506 Hz for (b)–(d). The output source array has a fixed momentum $k_z = \frac{\pi}{2d_z}$.

acoustic lattice with direct printing. A full picture of our sample is shown in Fig. 3(a), and the inset shows the enlarged view of the A/B meta-atoms (see details in Supplemental Material Secs. 13 and 15 [55]). First, in Figs. 3(c)–3(f), we show the topological propagation of the edge states at point X with $\phi = \frac{\pi}{2}$ and $m = 0$. The schematic speakers point out the positions of the source array that can emit acoustic waves with a frequency of 11 718 Hz within the topological bandwidth ranging from 11 109 Hz to 11 934 Hz (Supplemental Material Sec. 16 [55]) and a fixed momentum $k_z = \frac{\pi}{2d_z}$, which indicates the acoustic waves move not only in the xy plane, but also in the z plane (Supplemental Material Sec. 13 [55]). After three- and five-layer propagation [Figs. 3(c) and 3(d)], we observe that the acoustic wave propagates along the external edge without penetrating into the interior of the fractal lattice and without backscattering when encountering the sharp corner. Moving the sound source leftward makes the acoustic wave propagate through the obtuse corner and farther down along the edge, as shown in Figs. 3(e) and 3(f). The same behavior is observed for the edge states localized at the internal edges, as shown in Figs. 3(g) and 3(h). Note that because of the lossy nature of sound, the energy dissipation after propagating through each layer is about 33% and the field intensity is renormalized to the maximum value at each layer.

Furthermore, attributed to the topological protection, the acoustic wave should propagate around the defect without backscattering. We block one cavity at the position indicated by the blue arrows in Figs. 3(i) and 3(j), then we use the same method as shown in Figs. 3(c) and 3(d) to carry out the experiment. Clearly, we observe that the acoustic wave moves along the edge, encounters the top corner and defect, and then continues moving downward along the left edge without backscattering. We notice that around the defect where the self-similarity is broken, the acoustic wave moves along a single-atom path, which pushes the robust propagation into the single-atom level. In Supplemental Material Sec. 17 [55], we also show in simulations that the waves can propagate around the defects located at different positions.

Contrary to the topological transmission displayed earlier, we experimentally observe that the propagation of the acoustic waves at trivial point Y, with $\phi = \frac{\pi}{2}$ and $m = 3.6t_2$, displays trapped behaviors. In Fig. 4(a), the numerical energy spectrum corresponding to point Y within the trivial regime includes no topological edge states. Note that in Supplemental Material Fig. S9 [55], we plot the field intensities of the suspicious edge states with the state number of 175 with an energy of -0.88 and the state number of 176 with an energy of -0.83. The dynamical simulations show the states can penetrate into the interior of the fractal lattice, and these states are not topologically protected (Supplemental Material Videos S7 and S8 [55]). The onsite energy difference m between the A and B sublattices is introduced by simply tuning the height of the sound cavities (Supplemental Material Sec. 18 [55]). After five-layer propagation, as shown in Figs. 4(b) and 4(c), we can see that the acoustic waves penetrate into the interior of the sample and scatter at the corners, as the source moves from the upper right edge to the lower left edge. The operating frequency is 10 506 Hz, corresponding to the energy of the suspicious edge states. The trapped behavior is also observed for sound propagating along the perimeter of the center void [Fig. 4(d)], which is in sharp contrast to the result shown in Fig. 3(h). Combined with the results at point X as shown in Fig. 3, we have experimentally verified that introducing the fractal lattice into the topological Haldane model retains the topological phase transitions, whereas the topological phase diagram is compressed.

IV. CONCLUSIONS

In summary, we have reported the observation of an acoustic Chern fractal insulator. The self-similar energy spectra and topological protection by a mobility gap instead of a direct bandgap made our fractal model distinct from conventional topological insulators. We investigated the interplay between the fractality and topological Haldane model, and pinpointed

that the phase diagram is significantly compressed and the energy spectra are in the form of a devil's staircase. In experiments, we confirmed the diagram squeezing and observed the robust propagation along the outer and inner edges of the fractal lattice. Our work paves the way to exploring further the interplay between fractality [48] and non-Hermitian physics [57–59], and shows potential in sensors [60] and robust networks [61].

ACKNOWLEDGEMENTS

This research is supported by the National Key Research and Development Program of China (Grants No. 2022YFA1404203 and No. 2022YFA1405200), the National Natural Science Foundation of China (Grants No. 12174339 and No. 12174340), and the Zhejiang Provincial Natural Science Foundation of China (Grant No. LR23A040003).

[1] M. Z. Hasan and C. L. Kane, Colloquium: Topological insulators, Rev. Mod. Phys. **82**, 3045 (2010).

[2] X. L. Qi and S. C. Zhang, Topological insulators and superconductors, Rev. Mod. Phys. **83**, 1057 (2011).

[3] F. D. M. Haldane, Model for a Quantum Hall Effect without Landau Levels: Condensed-Matter Realization of the Parity Anomaly, Phys. Rev. Lett. **61**, 2015 (1988).

[4] D. J. Thouless, M. Kohmoto, M. P. Nightingale, and M. den Nijs, Quantized Hall Conductance in a Two-Dimensional Periodic Potential, Phys. Rev. Lett. **49**, 405 (1982).

[5] R. Yu, W. Zhang, H.-J. Zhang, S.-C. Zhang, X. Dai, and Z. Fang, Quantized anomalous Hall effect in magnetic topological insulators, Science **329**, 61 (2010).

[6] C. Z. Chang *et al.*, Experimental observation of the quantum anomalous Hall effect in a magnetic topological insulator, Science **340**, 167 (2013).

[7] F. D. M. Haldane and S. Raghu, Possible Realization of Directional Optical Waveguides in Photonic Crystals with Broken Time-Reversal Symmetry, Phys. Rev. Lett. **100**, 013904 (2008).

[8] Z. Wang, Y. D. Chong, J. D. Joannopoulos, and M. Soljačić, Reflection-free One-Way Edge Modes in a Gyromagnetic Photonic Crystal, Phys. Rev. Lett. **100**, 013905 (2008).

[9] Z. Wang, Y. Chong, J. D. Joannopoulos, and M. Soljačić, Observation of unidirectional backscattering-immune topological electromagnetic states, Nature (London) **461**, 772 (2009).

[10] M. C. Rechtsman, J. M. Zeuner, Y. Plotnik, Y. Lumer, S. Nolte, M. Segev, and A. Szameit, Photonic Floquet topological insulators, Nature (London) **496**, 196 (2012).

[11] K. Fang, Z. Yu, and S. Fan, Realizing effective magnetic field for photons by controlling the phase of dynamic modulation, Nat. Photonics **6**, 782 (2012).

[12] M. Hafezi, S. Mittal, J. Fan, A. Migdall, and J. M. Taylor, Imaging topological edge states in silicon photonics, Nat. Photonics **7**, 1001 (2013).

[13] T. Ozawa, H. M. Price, A. Amo, N. Goldman, M. Hafezi, L. Lu, M. C. Rechtsman, D. Schuster, J. Simon, O. Zilberberg, and I. Carusotto, Topological photonics, Rev. Mod. Phys. **91**, 015006 (2019).

[14] A. B. Khanikaev, S. Hossein Mousavi, W.-K. Tse, M. Kargarian, A. H. MacDonald, and G. Shvets, Photonic topological insulators, Nat. Mater. **12**, 233 (2013).

[15] A. B. Khanikaev, R. Fleury, S. H. Mousavi, and A. Alù, Topologically robust sound propagation in an angular-momentum-biased graphene-like resonator lattice, Nat. Commun. **6**, 8260 (2015).

[16] X. Ni, C. He, X. C. Sun, X. P. Liu, M. H. Lu, L. Feng, and Y. F. Chen, Topologically protected one-way edge mode in networks of acoustic resonators with circulating air flow, New J. Phys. **17**, 053016 (2015).

[17] M. Xiao, W.-J. Chen, W.-Y. He, and C. T. Chan, Synthetic gauge flux and Weyl points in acoustic systems, Nat. Phys. **11**, 920 (2015).

[18] Z. Yang, F. Gao, X. Shi, X. Lin, Z. Gao, Y. Chong, and B. Zhang, Topological Acoustics, Phys. Rev. Lett. **114**, 114301 (2015).

[19] P. Roux, J. de Rosny, M. Tanter, and M. Fink, The Aharonov-Bohm Effect Revisited by an Acoustic Time-Reversal Mirror, Phys. Rev. Lett. **79**, 3170 (1997).

[20] Y. Ding, Y. Peng, Y. Zhu, X. Fan, J. Yang, B. Liang, X. Zhu, X. Wan, and J. Cheng, Experimental Demonstration of Acoustic Chern Insulators, Phys. Rev. Lett. **122**, 014302 (2019).

[21] F. Li, X. Huang, J. Lu, J. Ma, and Z. Liu, Weyl points and Fermi arcs in a chiral phononic crystal, Nat. Phys. **14**, 30 (2018).

[22] H. Ge, X. Ni, Y. Tian, S. K. Gupta, M.-H. Lu, X. Lin, W.-D. Huang, C. T. Chan, and Y.-F. Chen, Experimental Observation of Acoustic Weyl Points and Topological Surface States, Phys. Rev. Appl. **10**, 014017 (2018).

[23] G. Ma, M. Xiao, and C. T. Chan, Topological phases in acoustic and mechanical systems, Nat. Rev. Phys. **1**, 281 (2019).

[24] X. Zhang, M. Xiao, Y. Cheng, M. H. Lu, and J. Christensen, Topological sound, Commun. Phys. **1**, 97 (2018).

[25] M. Xiao, G. Ma, Z. Yang, P. Sheng, Z. Q. Zhang, and C. T. Chan, Geometric phase and band inversion in periodic acoustic systems, Nat. Phys. **11**, 240 (2015).

[26] H. Nassar, B. Yousefzadeh, R. Fleury, M. Ruzzene, A. Alù, C. Daraio, A. N. Norris, G. Huang, and M. R. Haberman, Nonreciprocity in acoustic and elastic materials, Nat. Rev. Mater. **5**, 667 (2020).

[27] S. Roman and D. H. Sebastian, Observation of phononic helical edge states in a mechanical topological insulator, Science **349**, 47 (2015).

[28] C. He, X. Ni, H. Ge, X. C. Sun, Y. B. Chen, M. H. Lu, X. P. Liu, and Y. F. Chen, Acoustic topological insulator and robust one-way sound transport, Nat. Phys. **12**, 1124 (2016).

[29] J. Lu, C. Qiu, L. Ye, X. Fan, M. Ke, F. Zhang, and Z. Liu, Observation of topological valley transport of sound in sonic crystals, Nat. Phys. **13**, 369 (2017).

[30] X. Cai, L. Ye, C. Qiu, M. Xiao, R. Yu, M. Ke, and Z. Liu, Symmetry-enforced three-dimensional Dirac phononic crystals, Light Sci. Appl. **9**, 38 (2020).

[31] B. Xie, H. X. Wang, X. Zhang, P. Zhan, J. H. Jiang, M. Lu, and Y. Chen, Higher-order band topology, Nat. Rev. Phys. **3**, 520 (2021).

[32] X. Ni, M. Weiner, A. Alù, and A. B. Khanikaev, Observation of higher-order topological acoustic states protected by generalized chiral symmetry, Nat. Mater. **18**, 113 (2019).

[33] Y. Qi, C. Qiu, M. Xiao, H. He, M. Ke, and Z. Liu, Acoustic Realization of Quadrupole Topological Insulators, Phys. Rev. Lett. **124**, 206601 (2020).

[34] H. Xue, Y. Yang, G. Liu, F. Gao, Y. Chong, and B. Zhang, Realization of an Acoustic Third-Order Topological Insulator, Phys. Rev. Lett. **122**, 244301 (2019).

[35] L. Luo, H. X. Wang, Z. K. Lin, B. Jiang, Y. Wu, F. Li, and J. H. Jiang, Observation of a phononic higher-order Weyl semimetal, Nat. Mater. **20**, 794 (2021).

[36] H. Qiu, M. Xiao, F. Zhang, and C. Qiu, Higher-Order Dirac Sonic Crystals, Phys. Rev. Lett. **127**, 146601 (2021).

[37] H. Xue, Y. Yang, F. Gao, Y. Chong, and B. Zhang, Acoustic higher-order topological insulator on a kagome lattice, Nat. Mater. **18**, 108 (2019).

[38] B. Jiang, A. Bouhon, Z.-K. Lin, X. Zhou, B. Hou, F. Li, R.-J. Slager, and J.-H. Jiang, Experimental observation of non-Abelian topological acoustic semimetals and their phase transitions, Nat. Phys. **17**, 1239 (2021).

[39] Q. Guo, T. Jiang, R. Y. Zhang, L. Zhang, Z. Q. Zhang, B. Yang, S. Zhang, and C. T. Chan, Experimental observation of non-Abelian topological charges and edge states, Nature (London) **594**, 195 (2021).

[40] O. You, S. Liang, B. Xie, W. Gao, W. Ye, J. Zhu, and S. Zhang, Observation of Non-Abelian Thouless Pump, Phys. Rev. Lett. **128**, 244302 (2022).

[41] D. J. Apigo, W. Cheng, K. F. Dobiszewski, E. Prodan, and C. Prodan, Observation of Topological Edge Modes in a Quasiperiodic Acoustic Waveguide, Phys. Rev. Lett. **122**, 095501 (2019).

[42] Z. G. Song, Y. Y. Zhang, and S. S. Li, The topological insulator in a fractal space, Appl. Phys. Lett. **104**, 233106 (2014).

[43] S. Pai and A. Prem, Topological states on fractal lattices, Phys. Rev. B **100**, 155135 (2019).

[44] A. A. Iliasov, M. I. Katsnelson, and S. Yuan, Hall conductivity of a Sierpiński carpet, Phys. Rev. B **101**, 045413 (2020).

[45] M. Fremling, M. van Hooft, C. M. Smith, and L. Fritz, Existence of robust edge currents in Sierpiński fractals, Phys. Rev. Res. **2**, 013044 (2020).

[46] Z. Yang, E. Lustig, Y. Lumer, and M. Segev, Photonic Floquet topological insulators in a fractal lattice, Light Sci. Appl. **9**, 128 (2020).

[47] M. N. Ivaki, I. Sahlberg, K. Pöyhönen, and T. Ojanen, Topological random fractals, Commun. Phys. **5**, 327 (2022).

[48] C. Sparrow and B. Mandelbrot, *The Fractal Geometry of Nature* (W. H. Freeman, New York, 1984).

[49] J.-F. Gouyet and A. L. R. Bug, *Physics and Fractal Structures* (Springer, New York, 1996).

[50] C. Liu, Y. Zhou, G. Wang, Y. Yin, C. Li, H. Huang, D. Guan, Y. Li, S. Wang, H. Zheng, C. Liu, Y. Han, J. W. Evans, F. Li, and J. Jia, Sierpiński Structure and Electronic Topology in Bi Thin Films on InSb(111)B Surfaces, Phys. Rev. Lett. **126**, 176102 (2021).

[51] T. Biesenthal, L. J. Maczewsky, Z. Yang, M. Kremer, M. Segev, A. Szameit, and M. Heinrich, Fractal photonic topological insulators, Science **376**, 1114 (2022).

[52] P. Titum, N. H. Lindner, M. C. Rechtsman, and G. Refael, Disorder-Induced Floquet Topological Insulators, Phys. Rev. Lett. **114**, 056801 (2015).

[53] X. S. Wang, A. Brataas, and R. E. Troncoso, Bosonic Bott Index and Disorder-Induced Topological Transitions of Magnons, Phys. Rev. Lett. **125**, 217202 (2020).

[54] P. Bak, The devil's staircase, Phys. Today **39**(12), 38 (1986).

[55] See Supplemental Material at http://link.aps.org/supplemental/10.1103/PhysRevResearch.5.023189 for (1) the method to calculate fractal dimension, Bott index, and cantor function; (2) the discussion for more states, more lattices, the validity of phase diagram and the robustness of the system; (3) finite-element simulation of acoustic fractal lattices.

[56] J. Li, Q. Mo, J. H. Jiang, and Z. Yang, Higher-order topological phase in an acoustic fractal lattice, Sci. Bull. (Beijing) **67**, 2040 (2022).

[57] E. J. Bergholtz, J. C. Budich, and F. K. Kunst, Exceptional topology of non-Hermitian systems, Rev. Mod. Phys. **93**, 015005 (2021).

[58] B. Hu, Z. Zhang, H. Zhang, L. Zheng, W. Xiong, Z. Yue, X. Wang, J. Xu, Y. Cheng, X. Liu, and J. Christensen, Non-Hermitian topological whispering gallery, Nature (London) **597**, 655 (2021).

[59] K. Wang, A. Dutt, C. C. Wojcik, and S. Fan, Topological complex-energy braiding of non-Hermitian bands, Nature (London) **598**, 59 (2021).

[60] J. C. Budich and E. J. Bergholtz, Non-Hermitian Topological Sensors, Phys. Rev. Lett. **125**, 180403 (2020).

[61] Z. Zhang, P. Delplace, and R. Fleury, Superior robustness of anomalous non-reciprocal topological edge states, Nature (London) **598**, 293 (2021).